COMSOL
CONFERENCE
2023 MUNICH

Optimal Design of Baking Plates for an Inductive Wafer Baking Oven

J. Steinbach[1], L. Jadachowski[1,2], A. Kugi[1,3], A. Steinboeck[1,2]
1. Automation and Control Institute, TU Wien, Vienna, Austria.
2. Christian Doppler Laboratory for Intelligent Process Control for High-Quality Steel Products, Automation and Control Institute, TU Wien, Vienna, Austria.
3. Austrian Institute of Technology (AIT), Vienna, Austria.

Abstract
A finite-element model of a baking plate pair used in an inductively heated wafer baking oven is derived and used for design optimization. Based on frequency-domain analyses of the electromagnetic field, the heat source generated by induced currents is approximated. This reduces the computational complexity by eliminating the need for coupled simulations. A nonlinear description of phase transformations in the batter, mainly the vaporization of water, is compared to a linearized approach. The antagonistic objectives of good temperature homogeneity and fast startup time of the oven lead to a tradeoff for the baking plate thickness. For a simple objective function, the optimal baking plate thickness is calculated explicitly by relations obtained from FEM simulations.

Keywords: Process control, Induction heating, Optimal design, Parametric optimization.

Introduction
Baking is a central production step in the industrial production of edible wafers and waffles. The liquid batter is heated between a pair of metallic baking plates. Establishing a uniform and accurate temperature at the baking face (inner baking plate surface) is crucial for product quality.

In traditional gas-fired ovens, the baking plates are heated by an array of gas burners. Recent developments aim at a technology transition to inductive heating ovens. Their main advantages are the absence of flue gas and increased efficiency [1]. However, the highly localized heat input into the baking plates and restrictions concerning the positions of inductors can lead to non-uniform temperature profiles in the baking plates and inhomogeneous product properties.

A COMSOL multiphysics finite-element model (FEM) serves to identify crucial design parameters and develop strategies that ensure the desired product quality. The analyzed problem involves induction heating, phase changes, conductive, convective, and radiative heat transfer. A computationally less expensive model is derived and expressed via the *Heat Transfer in Solids* module to reduce the computational effort. The 2D simulation domain (yz-plane) represents a cross-section of the baking plate, see Figure 1. Temperature uniformity is assumed along the x-direction (normal to the cross-section, motion direction). Figure 1 shows the basic geometry of the baking plates and inductors.

The baking plate pairs travel cyclically through the oven. At one position along this path, finished products are extracted and new batter is deposited. The cycle time of this process is t_c.

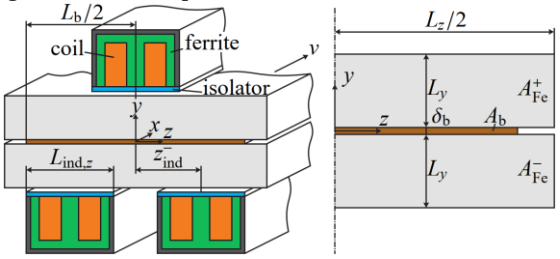

Figure 1. Setup of the FEM simulation. The left part shows the physical setup used to determine the electromagnetic heat source. The right part shows the domain of the computational model in the yz-plane.

The paper's main contribution is optimizing the baking plate thickness L_y based on FEM simulations. An increased baking plate thickness is hypothesized to reduce temperature variations at the baking face, where the baking plates are in contact with the batter. However, thicker baking plates have higher thermal capacities and require longer to reach the desired operating temperature after start-up from ambient temperature.

Finite Element Model
This section is organized in three parts: 1) geometry of the setup and heat equation, 2) characterization of inductive heat sources, and 3) models of the baking process. Three simulations are discussed in this work: A, a steady-state simulation using averaged quantities; B, a time dependent study with a nonlinear baking process model; C, a time-dependent study with a linear baking process model.

Heat equation
The temperature is assumed to be homogeneous in the traveling direction of the baking plates (x-direction, L_x is the baking plate length). Because the leading and trailing faces of the baking plates mainly exchange heat with the leading/trailing faces of other baking plates with similar temperatures,

gradients along this direction are expected to be negligible. The batter deposition is usually centered on the baking face, and the batter covers a significant fraction of this area. The distance δ_b between the lower and upper plate equals the batter thickness.

The baking plate thickness is L_y, and the width is L_z. For symmetry reasons, only $z \in [0, L_z/2]$ is considered in the computational model. Note that the y-dimension of the geometry setup is formed by two baking plate thicknesses L_y and the gap width δ_b. The heat equation for the 2-dimensional problem within the domains $A_i \in \{A_\mathrm{Fe}^\pm, A_\mathrm{b}\}$ (see Figure 1) with material properties ρ (mass density), c_p (specific heat capacity, possibly depending on T), and λ (heat conductance) not explicitly depending on (y,z) reads as

$$\rho c_\mathrm{p}(T)\frac{\partial T}{\partial t}(y,z,t) = \lambda\left(\frac{\partial^2 T}{\partial y^2}(y,z,t) + \frac{\partial^2 T}{\partial z^2}(y,z,t)\right) + Q(y,z,t) \quad (1)$$

together with the initial condition

$$T(y,z,t_0) = T_0(y,z) \quad \text{for} \quad (y,z) \in A_i. \quad (1a)$$

The source term $Q(y,z,t)$ is represents the inductive power and the necessary heat for the linear baking process model (simulations A and C). The appropriate boundary conditions on $(y,z) \in \partial A_i$ are given by Neumann boundary conditions

$$-n_y\lambda\frac{\partial T}{\partial y}(y,z,t) - n_z\lambda\frac{\partial T}{\partial z}(y,z,t) = q_n(T,y,z,t), \quad (1b)$$

where n_y and n_z are the components of the unit normal surface vector and q_n is the normal heat flux leaving the surface. At the symmetry axis ($z = 0$), $q_n = 0$ follows. The same was assumed for the boundary between the batter and the air in the gap between the baking plates since the main heat transfer happens via the baking plates.

The heat flows corresponding to the boundaries of the baking plate at $y = \pm\left(L_y + \frac{\delta_\mathrm{b}}{2}\right)$ and $z = \frac{L_z}{2}$ are based on the sum of radiative heat exchange and the lumped-parameter heat exchange coefficients identified in [2] from measurements at the industrial plant. Heat transfer between the lower and upper baking plate in the small section without batter was modeled by air-gap conductance and radiative heat exchange.

A constant contact resistance models the contact between the batter and the baking plates. The value of the corresponding specific heat exchange coefficient mainly affects the duration during of liquid water in the batter domain, i.e. its temperature is at 100 °C. This specific heat transfer coefficient was chosen such that this duration (transient simulation C, nonlinear $c_\mathrm{p}(T)$) approximately meets the operator-observed vaporization duration t_b of the "hissing phase" [1].

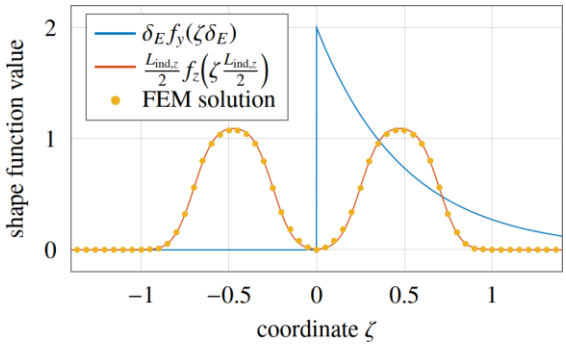

Figure 2. Shape functions f_y and f_z in normalized form. $L_{ind,z}$ is the inductor width and δ_E is the penetration depth of the electromagnetic field. Note that the normalization constants have very different orders of magnitude $\left(\delta_E \ll \frac{L_{ind,z}}{2}\right)$.

A constant specific heat capacity c_p was used for the baking plates. The material properties ρ and λ of the baking plates were taken from typical values of cast gray iron [3].

Inductive Heat Sources

The spatial distribution of the inductive heating power has been obtained based on electromagnetic simulations and theoretical considerations. In order to keep the computational effort low, this identified spatial distribution was used instead of repeated electromagnetic FEM simulations. The inductive heating power is thus represented by a volumetric heat source

$$Q(y,z,t) = P_+(t)\frac{1}{L_+}f_y\left(L_y + \frac{\delta_\mathrm{b}}{2} - y\right)f_z(z)$$

within A_Fe^+ and

$$Q(y,z,t) = P_-(t)\frac{1}{L_-}f_y\left(L_y + \frac{\delta_\mathrm{b}}{2} + y\right)f_z(z - z_\mathrm{ind}^-)$$

within A_Fe^-. $P_+(t)$ $\left(P_-(t)\right)$ is the momentary power of the inductor heating the upper (lower) baking plate, and $1/L_+$ $(1/L_-)$ is a normalization factor to transform it into power per unit length. The average power over one baking cycle was used for the steady-state simulation A. The lateral distance of the inductor center from the symmetry line is z_ind^- for the lower baking plates and zero for the upper baking plates.

The functions $f_y(\cdot)$ and $f_z(\cdot)$ are shape functions satisfying the integral properties $\int_0^\infty f_y(y)\,\mathrm{d}y = 1$ and $\int_{-\infty}^\infty f_z(z)\,\mathrm{d}z = 1$. The shape functions are shown in Figure 2 in a normalized form. Within numerical accuracy, both shape functions do fulfill the integral properties for the relevant finite integral bounds, i.e. the baking plate dimensions. The shape function

$$f_y(y) = \begin{cases} \frac{2}{\delta_\mathrm{E}}e^{-2y/\delta_\mathrm{E}} & y > 0 \\ 0 & y \le 0 \end{cases}, \qquad \delta_\mathrm{E} = \sqrt{\frac{\rho_E}{\mu_E \pi f}}$$

is based on exponential decay and the electromagnetic field's penetration depth δ_E [4]. ρ_E is the electric resistivity of the material, μ_E is the

magnetic permeability, and f is the frequency of the electromagnetic field. An electromagnetic FEM solution with appropriate mesh element quality [5] and spatial resolution is of considerable computational complexity. Thus, $f_y(\cdot)$ is used. The shape function $f_z(z) = a\big(\mathrm{erf}(b|z| - c) - \mathrm{erf}(b|z| - d)\big)$ in z-direction is based on sigmoid functions. The location and scale parameters a, b, c, d were identified by the least-squares error method based on frequency-domain simulations.

Model of the Baking Process

The ratio $\frac{L_\mathrm{b}\delta_\mathrm{b}}{2L_yL_z}$ of the cross-sectional areas of the batter to the baking plates does not equal their volume ratios. The 2D FEM model entails a model-plant mismatch rectified using the mass density $\rho = \rho_\mathrm{w}\frac{V_\mathrm{b}}{L_\mathrm{b}\delta_\mathrm{b}L_x}$. Here, ρ_w is the mass density of water. V_b is the actual batter volume, and $L_\mathrm{b}\delta_\mathrm{b}L_x$ is its volume in the 2D FEM analysis. The thermal conductance λ of batter is assumed to be equal to that of liquid water. Due to the small δ_b, the influence of this parameter is negligible.

The energy needed to bake one wafer is given by the enthalpy difference ΔH between the raw batter and the finished product. In this work, all dry components are considered to have a common specific heat capacity c_d. The water content enters as mass fraction p_w, while c_w and c_v are the specific heat capacities of water and vapor. The latent heat of vaporization at temperature T_v is h_v. The initial temperature of the batter is T_0, and the product and the water vapor reach T_1 at the end of the baking process. The enthalpy difference is then given by

$$\Delta H = \rho_\mathrm{w}V_\mathrm{b}\big((1-p_\mathrm{w})c_\mathrm{d}(T_1 - T_0) + p_\mathrm{w}c_\mathrm{w}(T_\mathrm{v} - T_0) + p_\mathrm{w}c_\mathrm{v}(T_1 - T_\mathrm{v}) + p_\mathrm{w}h_\mathrm{v}\big). \quad (2)$$

For the steady-state simulation A, the energy ΔH has to be supplied each baking cycle with duration $\mathrm{t_c}$. Thus, a negative source term in the batter domain A_b is introduced: $Q = \frac{-\Delta H}{t_cL_\mathrm{b}\delta_\mathrm{b}L_x}$.

The transient simulation B uses a nonlinear model to approximate the baking process accurately. The specific heat capacity of the batter domain is temperature dependent and satisfies $\Delta H = \rho_\mathrm{w}V_\mathrm{b}\int_{T_0}^{T_1} c_\mathrm{p}(T)\,\mathrm{dT}$. In order to speed up simulations and to ensure a differentiable $c_\mathrm{p}(T)$, a smooth unit step function $\mathrm{st}(\cdot)$ as well as a smooth impulse $\mathrm{imp}(\cdot)$ function are used to approximate the impulse and step at T_v. Together with the heat capacities $c_{\mathrm{p},1}$ and $c_{\mathrm{p},2}$ at temperatures below and above T_v,

$$c_{\mathrm{p},1} = (1-p_\mathrm{w})c_\mathrm{d} + p_\mathrm{w}c_\mathrm{w}$$
$$c_{\mathrm{p},2} = (1-p_\mathrm{w})c_\mathrm{d} + p_\mathrm{w}c_\mathrm{v},$$

the expression for $c_\mathrm{p}(T)$ follows as

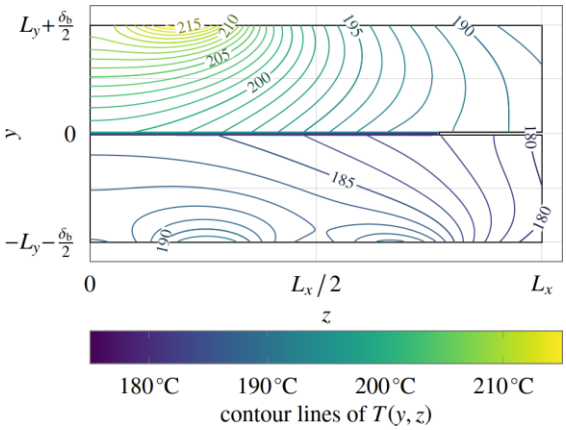

Figure 3. Steady-state temperature field in a typical baking plate. δ_b is the batter thickness.

$$c_\mathrm{p}(T) = c_{\mathrm{p},1}\mathrm{st}\left(\frac{T_\mathrm{v}-T}{\sigma_T}\right) + c_{\mathrm{p},2}\left(1 - \mathrm{st}\left(\frac{T_\mathrm{v}-T}{\sigma_T}\right)\right) + p_\mathrm{w}h_\mathrm{v}\mathrm{imp}\left(\frac{T-T_\mathrm{v}}{\sigma_T}\right).$$

Here, σ_T is a smoothening parameter. The functions $\mathrm{st}(\cdot)$ and $\mathrm{imp}(\cdot)$ satisfy $\int_{-\infty}^{\infty}\mathrm{imp}(\zeta)\,\mathrm{d}\zeta = 1$ and are based on Gaussian functions:

$$\mathrm{st}(\zeta) = \frac{1}{2}\big(1 + \mathrm{erf}(\zeta)\big) = \frac{1}{\sqrt{2\pi}}\int_{-\infty}^{\zeta} e^{-\frac{\eta^2}{2}}\,\mathrm{d}\eta,$$

$$\mathrm{imp}(\zeta) = \frac{1}{\sqrt{2\pi}}e^{-\frac{\zeta^2}{2}} = \frac{\mathrm{d}}{\mathrm{d}\zeta}\mathrm{st}(\zeta).$$

Further phase transitions like melting of fats or sugar can be considered in a similar way.

A linear batter model with the same qualitative behavior as the previous $c_\mathrm{p}(T)$ was developed and used in the transient simulation C. Here, $c_{\mathrm{p},1}$ is used as the constant specific heat capacity of the batter. To satisfy the energy balance, the source term $Q(y,z,t) = Q(t)$ in the batter domain is used to remove the enthalpy difference $\Delta H_\mathrm{C} = \Delta H - \rho_\mathrm{w}V_\mathrm{b}c_{\mathrm{p},1}(T_1 - T_0)$. Thus, in the transient simulation C, the source term $Q(t) = \frac{-\Delta H_\mathrm{C}}{t_\mathrm{b}L_\mathrm{b}\delta_\mathrm{b}L_x}$ for the time interval t_b of every cycle and $Q(t) = 0$ otherwise. The time t_b is the duration of the hissing phase.

The steady-state temperature field for a specific baking plate thickness is shown in Figure 3. The areas directly facing the inductors are warmer than the distant edges of the baking plates. This is more pronounced for the upper baking plate because the inductors are lined up here, while there are always two inductors in parallel for the bottom plates.

Optimization Problem

The antagonistic objectives of fast start-up times and low temperature variation can be balanced by weighting them according to their relative importance. We seek to minimize a cost function $C(L_y)$ that depends only on the scalar value of the baking plate thickness. It is based on the weighted sum $C(L_y) = C_t t_\mathrm{start}(L_y) + C_{T,t}T_{\Delta,\mathrm{t}}(L_y) + C_{T,z}T_{\Delta,\mathrm{z}}(L_y)$ where $C_t t_\mathrm{start}(L_y)$ is the cost related

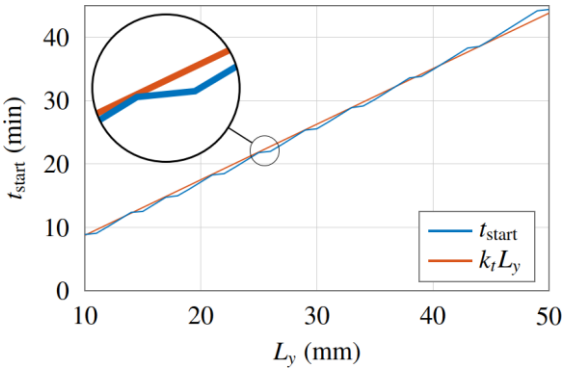

Figure 4. Start-up time t_{start} vs. baking plate thickness L_y and comparison with the linear approximation $k_t L_y$.

to the start-up time t_{start}, $C_{T,t}T_{\Delta,\text{t}}(L_y)$ is the cost related to the temporal temperature variation $T_{\Delta,\text{t}}(L_y)$, and $C_{T,z}T_{\Delta,\text{z}}(L_y)$ is the cost related to the spatial temperature variation $T_{\Delta,\text{z}}(L_y)$ along the z-direction. The positive values C_t, $C_{T,t}$, and $C_{T,z}$ control the relative importance of start-up time, temporal temperature variation and spatial temperature variation.

The start-up time t_{start} can be identified by transient simulations. It is defined here as the time when the spatially averaged temperature in the baking plates exceeds $T_1 = 185\ °\text{C}$ for the first time.

$$t_{\text{start}} = \min t \tag{3a}$$

$$\text{s.t.}\ \frac{\int_{A_{\text{Fe}}} T(y,z,t)\,\text{d}A}{\int_{A_{\text{Fe}}} \text{d}A} \geq T_1, \tag{3b}$$

$$A_{\text{Fe}} = A_{\text{Fe}}^{+} \cup A_{\text{Fe}}^{-}. \tag{3c}$$

The condition in (3) can only be satisfied if the temperature is rising, i.e., when the baking plate is under an inductor. Since these periods of time are spaced by the cycle time t_c, t_{start} can only have values from t_c-spaced intervals, leading to the nonsmooth shape in Figure 4. Put differently, a small increase of L_y either leads to a t_{start} within the same cycle (nearly unnoticeable increase of t_{start}) or to a t_{start} in the next cycle time, approximately increasing t_{start} by t_c. Since these discontinuities in $t_{\text{start}}(L_y)$ are different for almost all baking plates in the oven, using the linear approximation $t_{\text{start}} \approx k_t L_y$ instead of the FEM results is the more sensible choice.

Temporal temperature inhomogeneities are related to the temperature range the product experiences during baking. Spatial temperature inhomogeneities inevitably lead to uneven product quality, e.g., in browning and residual moisture. This work uses the temporal standard deviation of a scalar, time-variant temperature as a temporal inhomogeneity measure.

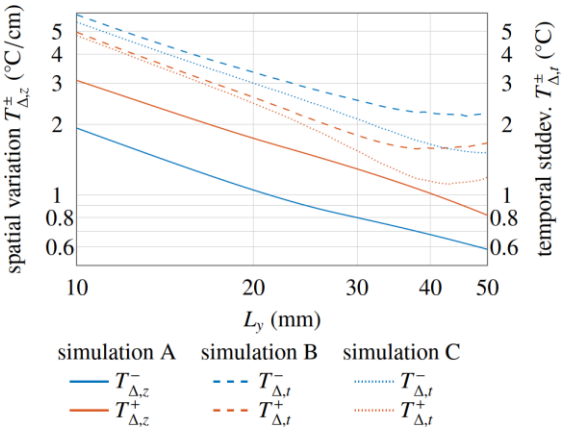

Figure 5. Temperature variations depending on the baking plate thickness L_y. Blue lines refer to the lower baking plates and orange lines to the upper baking plates.

The spatially averaged temperatures $T_{\text{f}}^{-}(t)$ and $T_{\text{f}}^{+}(t)$ of the lower baking face and the upper baking face, respectively, and their temporal standard deviation read as:

$$T_{\text{f}}^{\pm}(t) = \frac{2}{L_b}\int_0^{\frac{L_b}{2}} \lim_{\Delta\to 0^+} T\left(\pm\frac{\delta_{\text{b}}}{2} \pm \Delta, z, t\right) \text{d}z, \tag{4a}$$

$$\bar{T}_{\text{f}}^{\pm} = \frac{1}{nt_c}\int_{t_0}^{t_0+nt_c} T_{\text{f}}^{\pm}(t)\,\text{d}t, \tag{4b}$$

$$T_{\Delta,\text{t}}^{\pm} = \sqrt{\frac{1}{nt_c}\int_{t_0}^{t_0+nt_c} \left(T_{\text{f}}^{\pm}(t) - \bar{T}_{\text{f}}^{\pm}\right)^2 \text{d}t}\,. \tag{4c}$$

The limit for the y-coordinate is necessary due to the thermal contact resistance assumed between the batter and the baking plates. The integer n is the number of cycles used for arithmetic averaging.

The spatial inhomogeneity is assessed in this work based on the mean of the temperature gradient magnitude obtained in the steady-state scenario A:

$$T_{\Delta,\text{z}}^{\pm} = \frac{2}{L_b}\int_0^{\frac{L_b}{2}} \lim_{\Delta\to 0^+} \left|\frac{\partial}{\partial z} T\left(\pm\frac{\delta_y}{2} \pm \Delta, z\right)\right| \text{d}z\,. \tag{5}$$

Figure 5 shows the temperature variation depending on the baking plate thickness. All axes use a logarithmic scale. The temperature variations decrease with L_y, approximately proportional to $1/L_y$ over a wide range. The temporal standard deviations of the lower baking plates $T_{\Delta,\text{t}}^{-}$ consistently exceed those of the upper baking plates, while the spatially averaged gradient magnitude of the upper baking plates $T_{\Delta,\text{z}}^{+}$ is higher than $T_{\Delta,\text{z}}^{-}$. This can be attributed to the inductor layout (see Figure 1): Two inductors arranged in parallel lead to reduced gradients in z-direction. On the other hand, this arrangement increases the temporal variations since the inductive power is concentrated in a shorter time for the lower baking plates.

For large values of L_y, the temporal standard deviations flatten out or increase again. The deviation from the $1/L_y$-behavior is neglected in this work, i.e., the measures of the temperature variation can be approximated by $\frac{k_\Delta}{L_y}$, with a constant k_Δ for each measure.

The baking plate thickness is confined to the interval $[L_y^-, L_y^+]$, where L_y^- is the minimum length required for mechanical stability and L_y^+ is an upper bound associated with the maximum load of the transport mechanism. This work uses $[10\ \text{mm}, 50\ \text{mm}]$ as an admissible set for the baking plate thickness L_y.

The optimization problem can then be formulated as

$$L_y^* = \underset{L_y \in [L_y^-, L_y^+]}{\arg\min}\ C(L_y) \qquad (6)$$
$$\text{s.t. } t_{\text{start}} \quad \text{according to (3)}$$
$$T_{\Delta,\text{t}} = T_{\Delta,\text{t}}^+ + T_{\Delta,\text{t}}^- \quad \text{according to (4)}$$
$$T_{\Delta,z} = T_{\Delta,\text{z}}^+ + T_{\Delta,\text{z}}^- \quad \text{according to (5)}$$

The low dimension (scalar optimization variable L_y) and relatively high computational costs of the FEM analysis stimulated using the following solution strategy: Identify the influence of L_y on $C(L_y)$ from a few simulations, derive a computationally inexpensive surrogate function $C_s(L_y)$ that approximates $C(L_y)$ with sufficient accuracy, and minimize $C_s(L_y)$ instead of $C(L_y)$.

Results and Discussion

The discussed approximations of the temperature variations $T_{\Delta,\text{t}} = T_{\Delta,\text{t}}^+ + T_{\Delta,\text{t}}^-$ and $T_{\Delta,\text{z}} = T_{\Delta,\text{z}}^+ + T_{\Delta,\text{z}}^-$ can be expressed in the form $T_{\Delta,\text{t}} \approx \frac{k_{\Delta,\text{t}}^+}{L_y} + \frac{k_{\Delta,\text{t}}^-}{L_y} = \frac{k_{\Delta,\text{t}}}{L_y}$ and $T_{\Delta,\text{z}} \approx \frac{k_{\Delta,\text{z}}^+}{L_y} + \frac{k_{\Delta,\text{z}}^-}{L_y} = \frac{k_{\Delta,\text{z}}}{L_y}$ where the four different k_Δ are the constants used for the approximation. The compact notation of the surrogate cost function then follows as the convex function

$$C_s(L_y) = C_t k_t L_y + C_{T,t}\frac{k_{\Delta,\text{t}}}{L_y} + C_{T,z}\frac{k_{\Delta,\text{z}}}{L_y}.$$

The approximate solution to (6) is then given by

$$L_y^* \approx \underset{L_y \in [L_y^-, L_y^+]}{\arg\min}\ C_s(L_y), \qquad (7)$$

which can be explicitly calculated. The solution is given by $\sqrt{(C_{T,t}k_{\Delta,\text{t}} + C_{T,z}k_{\Delta,\text{z}})/(C_t k_t)}$ if it lies inside $[L_y^-, L_y^+]$, or its projection into the interval.

Figure 6 shows the cost function and its components, as well as their corresponding approximations for the following set of weights: $C_t = 1\,\frac{1}{\text{min}}$, $C_{T,t} = 5\,\frac{1}{°\text{C}}$ and $C_{T,z} = 5\,\frac{\text{cm}}{°\text{C}}$. In the shown example, simulation C was used for the temporal variations (using simulation B or the sum of both yields qualitatively equal results).

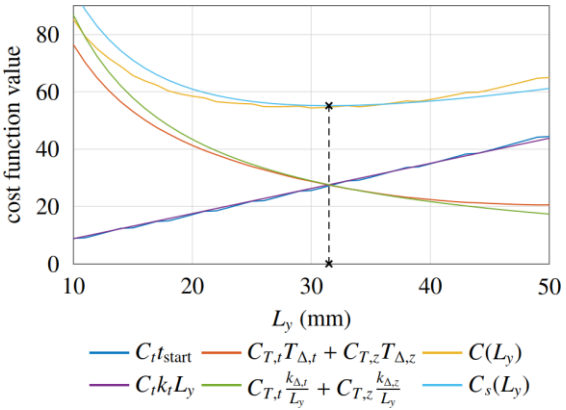

Figure 6. Cost function $C(L_y)$ and its components (top row of legend) and corresponding approximations (bottom row of legend). Simulation C was used for temporal temperature variations. The minimum (black x) was calculated based on the surrogate function.

Conclusions

A finite element model of a pair of baking plates used in an industrial wafer baking oven was derived, simplified, and used for design optimization in a computationally efficient way. Namely, the phase change of the batter and the inductive heating were modeled by their thermal effects alone, and the optimization problem was converted to a surrogate optimization. The computational costs of FEM simulations and the baking plate design optimization could be significantly reduced.

References

[1] K. Tiefenbacher, The Technology of Wafers and Waffles I: Operational Aspects, London: Academic Press, 2017.

[2] J. Steinbach, L. Jadachowski, A. Steinboeck and A. Kugi, "Modeling and Optimization of an Inductive Oven with Continuous Product Flow," *IFAC-PapersOnline*, vol. 55, no. 27, pp. 184-189, 2022.

[3] D. R. Lide, CRC Handbook of Chemistry and Physics, Boca Raton: CRC Press, 2004.

[4] S. Lupi, M. Forzan and A. Aliferov, Induction and Direct Resistance Heating - Theory and Numerical Modeling, Cham: Springer, 2015.

[5] COMSOL AB, COMSOL Multiphysics Reference Manual, Version 5.6, 2020.

Acknowledgements

Technical and financial Support by FHW Franz Haas Waffelmaschinen GmbH is gratefully acknowledged.